Hindawi
Geofluids
Volume 2018, Article ID 8217921, 16 pages
https://doi.org/10.1155/2018/8217921

Research Article

Experimental Study on Stress-Dependent Nonlinear Flow Behavior and Normalized Transmissivity of Real Rock Fracture Networks

Qian Yin,[1,2] **Hongwen Jing**,[1] **Richeng Liu**,[1] **Guowei Ma**,[2,3] **Liyuan Yu**,[1] **and Haijian Su**[1]

[1]*State Key Laboratory for Geomechanics and Deep Underground Engineering, China University of Mining and Technology, Xuzhou 221116, China*
[2]*School of Civil, Environmental and Mining Engineering, The University of Western Australia, Perth, WA 6009, Australia*
[3]*College of Architecture and Civil Engineering, Beijing University of Technology, Beijing 100124, China*

Correspondence should be addressed to Haijian Su; hjsu@cumt.edu.cn

Received 10 November 2017; Revised 25 February 2018; Accepted 15 March 2018; Published 24 April 2018

Academic Editor: Julie K. Pearce

The mechanism and quantitative descriptions of nonlinear fluid flow through rock fractures are difficult issues of high concern in underground engineering fields. In order to study the effects of fracture geometry and loading conditions on nonlinear flow properties and normalized transmissivity through fracture networks, stress-dependent fluid flow tests were conducted on real rock fracture networks with different number of intersections (1, 4, 7, and 12) and subjected to various applied boundary loads (7, 14, 21, 28, and 35 kN). For all cases, the inlet hydraulic pressures ranged from 0 to 0.6 MPa. The test results show that Forchheimer's law provides an excellent description of the nonlinear fluid flow in fracture networks. The linear coefficient a and nonlinear coefficient b in Forchheimer's law $J = aQ + bQ^2$ generally decrease with the number of intersections but increase with the boundary load. The relationships between a and b can be well fitted with a power function. A nonlinear effect factor $E = bQ^2/(aQ + bQ^2)$ was used to quantitatively characterize the nonlinear behaviors of fluid flow through fracture networks. By defining a critical value of $E = 10\%$, the critical hydraulic gradient was calculated. The critical hydraulic gradient decreases with the number of intersections due to richer flowing paths but increases with the boundary load due to fracture closure. The transmissivity of fracture networks decreases with the hydraulic gradient, and the variation process can be estimated using an exponential function. A mathematical expression $T/T_0 = 1 - \exp(-\alpha J^{-0.45})$ for decreased normalized transmissivity T/T_0 against the hydraulic gradient J was established. When the hydraulic gradient is small, T/T_0 holds a constant value of 1.0. With increasing hydraulic gradient, the reduction rate of T/T_0 first increases and then decreases. The equivalent permeability of fracture networks decreases with the applied boundary load, and permeability changes at low load levels are more sensitive.

1. Introduction

Rock fracture networks constitute the main pathways of fluid flow and solute migration in deep underground projects, and during the past several decades, substantial efforts have been devoted to the estimation of fluid flow behavior and transmissivity of fractures in many geoengineering and geosciences such as underground tunneling [1–3], CO_2 sequestration [4, 5], geothermal energy extraction [6–8], and hazardous wastes isolation [9–11]. The fluid flow in rock fractures is commonly assumed to follow the cubic law, in which the flow rate is linearly proportional to the pressure gradient [12–14]. However, when the flow rate/hydraulic head difference is large, deviation from the linear Darcy law may occur. In such case, the conductivity of the fractures calculated using the cubic law will be overestimated [15–17]. In addition, natural rock fractures are often characteristic of rough walls, intersections, and asperity contacts, which make the fluid flow process even more complex and difficult to accurately describe [18–22]. Therefore, a thorough understanding of

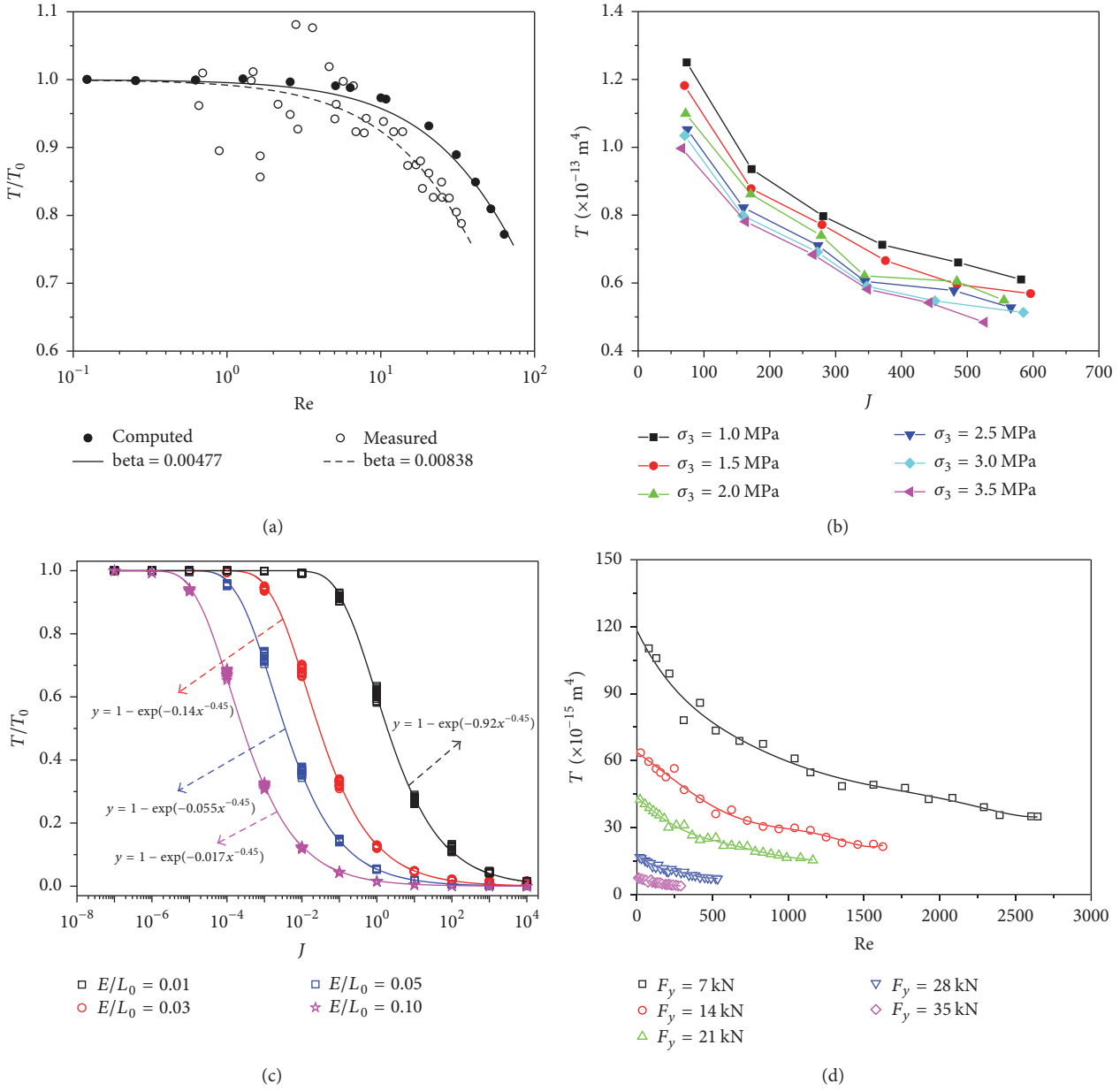

Figure 1: Relationships between hydraulic gradient J (Reynolds number Re) and the (normalized) transmissivity in previous studies. (a) Relationships between T/T_0 and Re (after [23]). (b) Relationships between T and J (after [24]). (c) Relationships between T/T_0 and J (after [14]). (d) Relationships between T and Re (after [25]).

nonlinear flow properties within fracture networks is of great significance to ensure performance and safety of engineering activities.

The transmissivity T, which is linked with volumetric flow rate, pressure gradient, and the fracture width, has been applied to characterize the onset of nonlinear flow regimes in rock fractures in some previous studies. Zimmerman et al. [23] conducted Navier-Stokes simulations and fluid flow tests in a natural 3D sandstone fracture and confirmed that weak inertia regimes exist for Reynolds number (Re) in the range of 1–10, where the fluid flow enters the nonlinear flow regime. The normalized transmissivity (T/T_0) remains constant when Re $<$ 1 but shows a decreasing trend when Re $=$ 1–10 (see Figure 1(a)). Zhang and Nemcik [24] experimentally investigated the fluid flow regimes through deformable rock fractures subjected to changing confining stress from 1.0 to 3.5 MPa. They found that for a nonmated sandstone fracture with the joint roughness coefficient of 9.2, the transmissivity is not a constant value but decreases with the hydraulic gradient J (see Figure 1(b)). Liu et al. [14] calculated the T/T_0-J curves of single fractures with various ratios of mechanical aperture to the fracture length, in which

the mechanical aperture is defined as the arithmetic average of the point-to-point distance between the two walls of a fracture. The results show that as J increases, T/T_0 decreases. When $J = 10^{-7}$–10^{-5}, T/T_0 remains constant approaching 1.0; the fluid flow is linear. For $10^{-4} < J < 10^{0}$, T/T_0 decreases dramatically; fluid flow enters a transitional regime. When $J > 10^{2}$, T/T_0 is sufficiently small and approaches 0; fluid flow enters a complete nonlinear regime (see Figure 1(c)). Yin et al. [25] estimated the relationships between T and Re for rough-walled fractures during shearing and subjected to various normal loads from 7 to 35 kN. As an example, for one of their samples with the shear displacement of 9 mm, T exhibits a decreasing trend with Re and the rate of its decrease diminishes. T as a function of Re can be well described using a six-order polynomial function (see Figure 1(d)). The above analysis generally focused on variations in (normalized) transmissivity of single fractures. However, when it comes to complex fracture networks, the stress-dependent nonlinear flow mechanisms and transmissivity are still not fully understood.

In engineering practices, both nature activities and human perturbations entail significant changes in the effective stress field of underground rock masses, which would then impact the fracture aperture in fracture networks. The void space between opposing surfaces can vary due to normal stress-induced closures or opening [18, 24, 26] or shear stress-induced dilations [27–29]. Hence, the fluid flow behavior and the transmissivity of rock fracture networks are stress-dependent, which has so far rarely been investigated.

The purpose of this paper is to investigate the stress-dependent nonlinear flow properties and normalized transmissivity of real rock fracture networks. First, plate granite specimens containing fracture networks with different number of intersections (1, 4, 7, and 12) were machined using a high-pressure water jet cutting system. Next, a series of high precision stress-dependent water flow tests with respect to different inlet hydraulic pressures ranging from 0 to 0.6 MPa and increasing applied boundary loads from 7 to 35 kN were conducted. The nonlinear flow behaviors, variations of the flow nonlinearity, normalized transmissivity and equivalent permeability of the fracture networks as a function of fracture networks geometry, and boundary load conditions were all examined.

2. Governing Equations of Fluid Flow in Fractures

Fluid flow through a single fracture is generally governed by the following Navier-Stokes (NS) equations, written in a tensor form as [15, 30, 31]:

$$\rho\left[\frac{\partial \mathbf{u}}{\partial t} + (\mathbf{u}\cdot\nabla)\,\mathbf{u}\right] = -\nabla p + \nabla\cdot\mathbf{T} + \rho\mathbf{f}, \tag{1}$$

where $\mathbf{u}$ is the flow velocity vector, p is the hydraulic pressure, $\mathbf{T}$ is the shear stress tensor, ρ is the fluid density, t is the time, $\mathbf{f}$ is the body force acting on the fluid, and in gravity environment $\mathbf{f}$ denotes the gravitational acceleration term.

For the case of incompressible and steady-state Newtonian flow, the terms involving time t drop out and the NS equations can be expressed as [1, 17]

$$\rho\,(\mathbf{u}\cdot\nabla)\,\mathbf{u} = -\nabla p + \mu\nabla^2\mathbf{u} + \mathbf{f}, \tag{2}$$

where μ is the dynamic viscosity.

Equation (2) is composed of a set of coupled nonlinear partial derivatives of varying orders. In order to solve these equations, an additional equation, called the mass conservation equation which can be achieved through mass continuity, is employed and the equation takes the form [1, 15]

$$\nabla\cdot\mathbf{u} = 0. \tag{3}$$

In (2), the convective acceleration term $(\mathbf{u}\cdot\nabla)\mathbf{u}$ denotes the inertial forces acting on the fluid, which are the source of nonlinearity [14]. The complexity of the Navier-Stokes equations makes exact solutions extremely difficult to achieve, especially for natural rock fractures with complicated geometries.

For certain cases with very low Reynolds number or flow rate, by assuming that the inertial forces of fluid flow through the fractures are negligible compared to the viscous forces. The convective acceleration term $(\mathbf{u}\cdot\nabla)\mathbf{u}$ in (2) vanishes, and the Navier-Stokes equations can be reduced to solvable forms as [12]

$$Q = -\frac{w{b_{\mathrm{h}}}^3}{12\mu}\nabla p, \tag{4}$$

where Q is the total volumetric flow rate, ∇p is the pressure gradient, w is the fracture width, and b_{h} is the hydraulic aperture. The flow rate is proportional to the cube of b_{h}. This equation is commonly referred to as the well-known cubic law.

The linear relation between Q and ∇p in (4) can only be anticipated for parallel-plate models under a limited range of flow rates. Besides, natural rock fractures are characterized by fracture intersections and complex fracture surface geometries, and the inertia items are often not zero. With increasing hydraulic head differences, the flow rate is nonlinearly related to the pressure drop and (4) is no longer applicable.

Some empirical expressions were proposed to describe the nonlinear flow in fractures, and Forchheimer's law is the most extensively used approach where the pressure gradient is a quadratic function of the flow rate, written as [32–34]

$$-\nabla P = a'Q + b'Q^2, \tag{5}$$

where a' and b' are model coefficients, representing pressure drop components caused by linear and nonlinear effects, respectively.

Since the hydraulic gradient J is proportional to ∇p as $J = \nabla p/(\rho g)$, (5) can then be written as follows:

$$J = aQ + bQ^2, \tag{6}$$

where $a = -\rho g a'$ and $b = -\rho g b'$.

The hydraulic gradient J is calculated by dividing the hydraulic head difference by the flow length

$$J = \frac{P}{\rho g L}, \tag{7}$$

where L is the flow length, which denotes the horizontal distance between the left and right specimen boundary in this study, and g is the gravitational acceleration.

To quantitatively estimate the nonlinearity of fluids flowing through the fracture networks, a nonlinear effect factor E was introduced to determine the fluid flow regime [1, 35, 36]. It can be presented by

$$E = \frac{bQ^2}{aQ + bQ^2}, \tag{8}$$

where aQ and bQ^2 are energy losses due to viscous and inertial dissipation mechanisms in the fractures. E denotes the ratio of nonlinear pressure drop to the overall pressure drop.

For engineering purposes, a critical value of $E = 10\%$ has been defined as the critical condition for onset of flow nonlinearity in fracture networks, where the nonlinear effect can be appreciable and cannot be neglected [23, 24, 29].

The Forchheimer number F_0 is another widely accepted parameter to characterize the onset of flow transition to nonlinearity, which is defined as the ratio of nonlinear to linear pressure drops [1, 13, 17],

$$F_0 = \frac{bQ^2}{aQ} = \frac{bQ}{a}. \tag{9}$$

Combinations of (8) and (9) yield the following equation:

$$E = \frac{F_0}{1 + F_0}. \tag{10}$$

Transmissivity (T) is an important hydraulic property to characterize the macroscopically observed flow resistances in fractures, which can be defined as [37]

$$-\nabla P = \frac{\mu Q}{Tw}. \tag{11}$$

When the flow rate is sufficiently low and the inertial forces are negligible, the intrinsic transmissivity (T_0) is commonly regarded as a constant value. As the hydraulic head difference increases, the transmissivity can be used to evaluate the nonlinear flow through the fractures, and the normalized transmissivity (T/T_0) was then determined [23],

$$\frac{T}{T_0} = \frac{-\mu Q/w\left(aQ + bQ^2\right)}{-\mu Q/w\,(aQ)} = 1 - E. \tag{12}$$

Therefore, as the nonlinear term (bQ^2) contributes to 10% of the total pressure drop or else $E = 10\%$, the critical value of T/T_0 is equal to 0.9. The corresponding J is defined as the critical hydraulic gradient J_c.

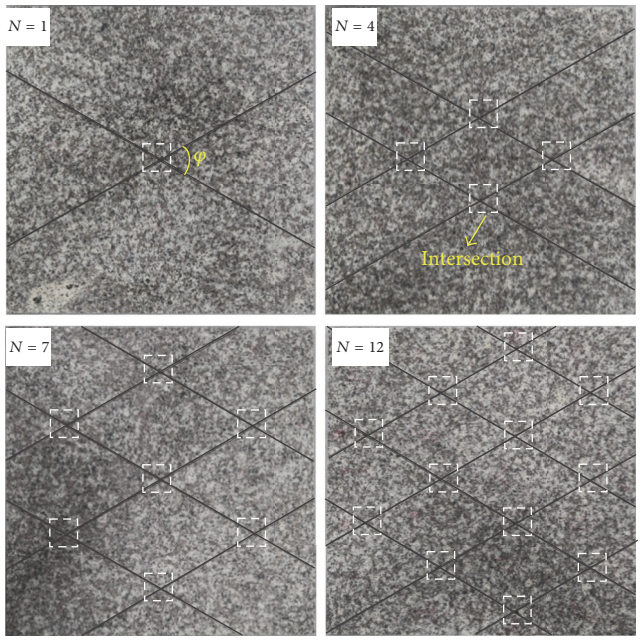

Figure 2: Plate granite specimens of fracture networks with different numbers of intersections ($N = 1$, 4, 7, and 12). The black lines denote the geometric locations the fractures.

3. Experimental Methodology

3.1. Rock Fracture Specimen Preparation. Granite specimens (495 × 495 × 17 mm in size) containing artificial fracture networks were established by using a high-pressure water jet cutting system [25]. The granites were taken from Linyi city in Shandong Province of China. The granite is a porphyritic monzonite with an average unit weight of about 2.69 g/cm^3. The uniaxial compressive strength of the rock is about 97.54 MPa, and its permeability is in the order of magnitude of 10^{-19} m^2.

The parallelism between the upper and lower surfaces of the plate specimens was controlled within an error of 0.02 mm. The water pressure of the water jet cutting system was held constant for all rock fractures, and the fractures penetrated the plate specimens thoroughly. Detailed descriptions of the rock fracture specimens are illustrated in Figure 2. Each specimen consists of two sets of parallel fractures with a constant included angle φ of 60°. By varying the spacing of the fractures, fracture networks with different numbers of intersections ($N = 1$, 4, 7, and 12) were, respectively, created.

Using a high-resolution three-dimensional laser scanning profilometer system, the fracture surface topography was measured before the hydromechanical tests. We considered the average of joint roughness coefficient (JRC) values for a series of 2D profiles along a fracture surface in the length direction, which is a suggested method by the International Society for Rock Mechanics and Rock Engineering (ISRM) to calculate the JRC of a 3D single fracture [38]. The spacing of 2D profiles is 3 mm. In total, the JRC values of 5 2D profiles are calculated and their average value is regarded as the JRC of a 3D single fracture. The JRC values of all 2D profiles were

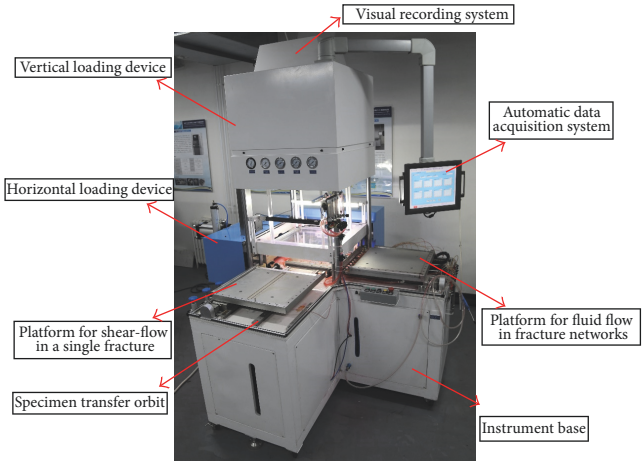

FIGURE 3: Schematic view of the stress-dependent fluid flow test apparatus.

estimated based on the values of Z_2 using (13) proposed by Tse and Cruden [39]. Here, JRC is a dimensionless index ranging from 1 to 20 [40], which has been widely accepted in the field of rock mechanics and rock engineering [22, 41].

The results indicate that JRC values of the fractures fluctuate within a very small range around 3.47. The fractures closely approximate parallel-plate models with a small JRC value.

$$Z_2 = \left[\frac{1}{M}\sum\left(\frac{z_{i-1} - z_i}{x_{i-1} - x_i}\right)^2\right]^{1/2} \quad (13)$$

$$\text{JRC} = 32.2 + 32.47 \log Z_2,$$

where x_i and z_i represent the coordinates of a fracture surface profile and M is the number of sampling points along the length of a fracture. Z_2 is the root mean square slope of the 2D profile.

3.2. Experimental Setup and Procedure. Before the hydromechanical tests, sealing of the fractured specimens was first conducted. Based on the model specimen size, a 3 mm thick rubber jacket was produced using the ethylene propylene diene monomer (EPDM) waterproof rubber [25]. Then, a rock fracture specimen was placed in the jacket, with the extra rubber seamlessly glued to the rock surface. For a better sealing of the fractures, a layer of glass glue was evenly coated on the specimen surface to leave the fractures open. Then, a piece of transparent crystal plate with a suitable size was attached to the glass glue. When the glass glue was dried, a hand-operated electric drill with a diameter of 10 mm was used to drill circular holes at the water inlet and outlet positions of the fractures through the rubber jacket. After a high-strength plexiglass cover plate and the horizontal load devices with uniform flow chambers were installed, the specimen was transferred to the test area.

The stress-dependent flow tests of the fracture networks were conducted by using a self-developed flow test apparatus [25], as shown in Figure 3. It mainly consists of three units: (i) *a platform for fluid flow in fracture networks*; (ii) *a water supply and measurement unit*; (iii) *a pneumatic-hydraulic cylinder unit*. During the flow tests, a constant water pressure was maintained at the flow inlet manifold using an air compressor connected to a water tank, with the pressure range of 0–2 MPa. Both water inlet directions (x- and y-directions) evenly featured 12 flow distribution chambers to achieve a variable but uniform flow field. The hydraulic sources of the water inlet or outlet manifold can be individually switched on or off using the shut-off valves (Figure 4(a)). Each of the 12 water chambers provided equal water pressure at the rock specimen boundary. The effluents flowing out of the fractures were measured in real time using four glass tube rotameters with a range of 0.0004–11.0 L/min. Both the horizontal (x- and y-directions) and vertical (z-direction) loads on the rock specimens were created using a pneumatic-hydraulic cylinder connected to an air compressor that has a maximum air pressure of 3 MPa. Before the test, a vertical load of 20 kN was applied on the specimen surface to balance the vertical water pressure in the fractures.

During the flow test, water was fed through the inflow manifold connected to a water tank that can supply a constant water head at all times by using an air compressor. Both horizontal boundary loads in the x-direction (F_x) and y-direction (F_y) were applied and increased from 7 to 35 kN in a 7 kN interval, with a fixed lateral pressure coefficient λ of F_y to F_x of 1.0. Applications of the boundary load conditions are displayed in Figure 4(b). In this study, we just discuss the x-directional nonlinear flow behaviors through the fracture networks over a range of inlet water pressures from 0 to 0.6 MPa with increasing boundary loads. To achieve this investigation, the side valves (x-direction) were opened while the top and bottom valves (y-direction) were closed, which forced water to flow horizontally from the right to left specimen boundary (x-direction) through the fracture networks. Other boundaries were considered impermeable.

For a certain boundary load and inlet hydraulic pressure, the total volume flow rate of the fracture networks at the water outlet boundary can be obtained when the glass rotor was relatively stable with no fluctuations. The effluent was then collected in another storage tank and recirculated. The entire hydraulic experiments were performed under isothermal conditions at room temperature of approximately 20°C. In addition, the fluid was assumed to be viscous with μ of 1.0 $\times 10^{-3}$ Pa·s and incompressible with ρ of 1000 kg/m^3.

4. Test Results and Discussion

Due to the low permeability of the intact granite matrix, fluid was assumed to flow through the fractures only during the hydromechanical tests. For the rock fracture specimen with various N subjected to different F (here, F refers to the boundary load due to $F_x = F_y$), a series of hydraulic tests were conducted with different inlet fluid pressures ranged from 0 to 0.6 MPa. In this study, the hydraulic head at the water outlet specimen boundary was assumed to be equal to zero. Thus, according to (7), in the range P of 0–0.6 MPa, J ranged from 0 to 123.69.

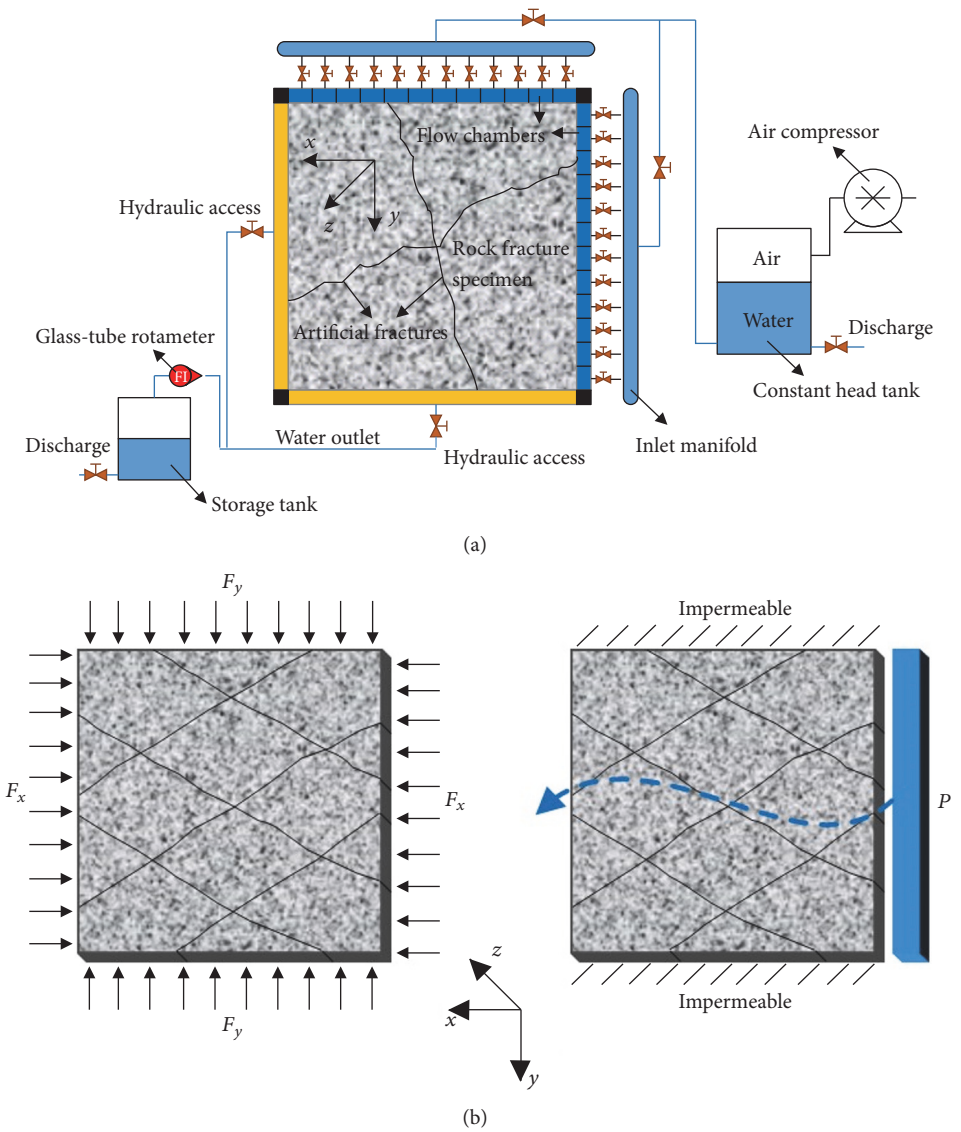

Figure 4: (a) A top view of hydraulic setup of the test apparatus. (b) Loading diagram of the rock fracture specimen.

The experimental data obtained in the hydraulic tests on the rock fracture specimens in the form of hydraulic gradient (J) versus discharge (Q) curves are displayed in Figure 5. The quadratic polynomial regression of Forchheimer (6) is used to best fit the raw experimental data, with the residual squared R^2 values all larger than 0.99 (Table 1). From Figure 5, with an increase in J, Q shows an increasing trend. For a certain N, as F increases, the slope of J-Q curves becomes steeper, indicating a higher flow resistance mainly as a result of fracture closure. Hence, more flow energy is required to achieve the same flow rate for fracture networks subjected to a larger boundary load. However, at a given F, as N increases, Q flowing out of the fracture networks produced by an identical hydraulic head shows an increasing trend (Figure 6). Taking F = 14 kN as an example, Q produced by J = 123.69 is increased from 5.04×10^{-6} m^3/s (N = 1) to 10.86×10^{-6} m^3/s (N = 12), increasing by approximately a factor of 1.15. With an increase in N, the overall discharge capacity of the fracture networks enhances.

The regression linear and nonlinear coefficients a and b in Forchheimer (6) for all test cases were then calculated and tabulated in Table 1. Figures 7(a)–7(d) show the variations of the coefficients a and b in terms of N and F. For a certain N, as F increases, both a and b show an increasing trend. In the range of F from 7 to 35 kN, a increases by 7.10–13.99 times and b increases by 3.97–7.73 times. The increase of coefficient a value is due to fracture closure induced by the boundary loads. However, for a certain F, as N increases, both a and b decrease. The variation process can be divided into two stages. For N = 1–7, the coefficients decrease significantly as N varies. However, in the range of 7–12, the coefficients vary gradually and approach essentially constant values. Using coefficient b

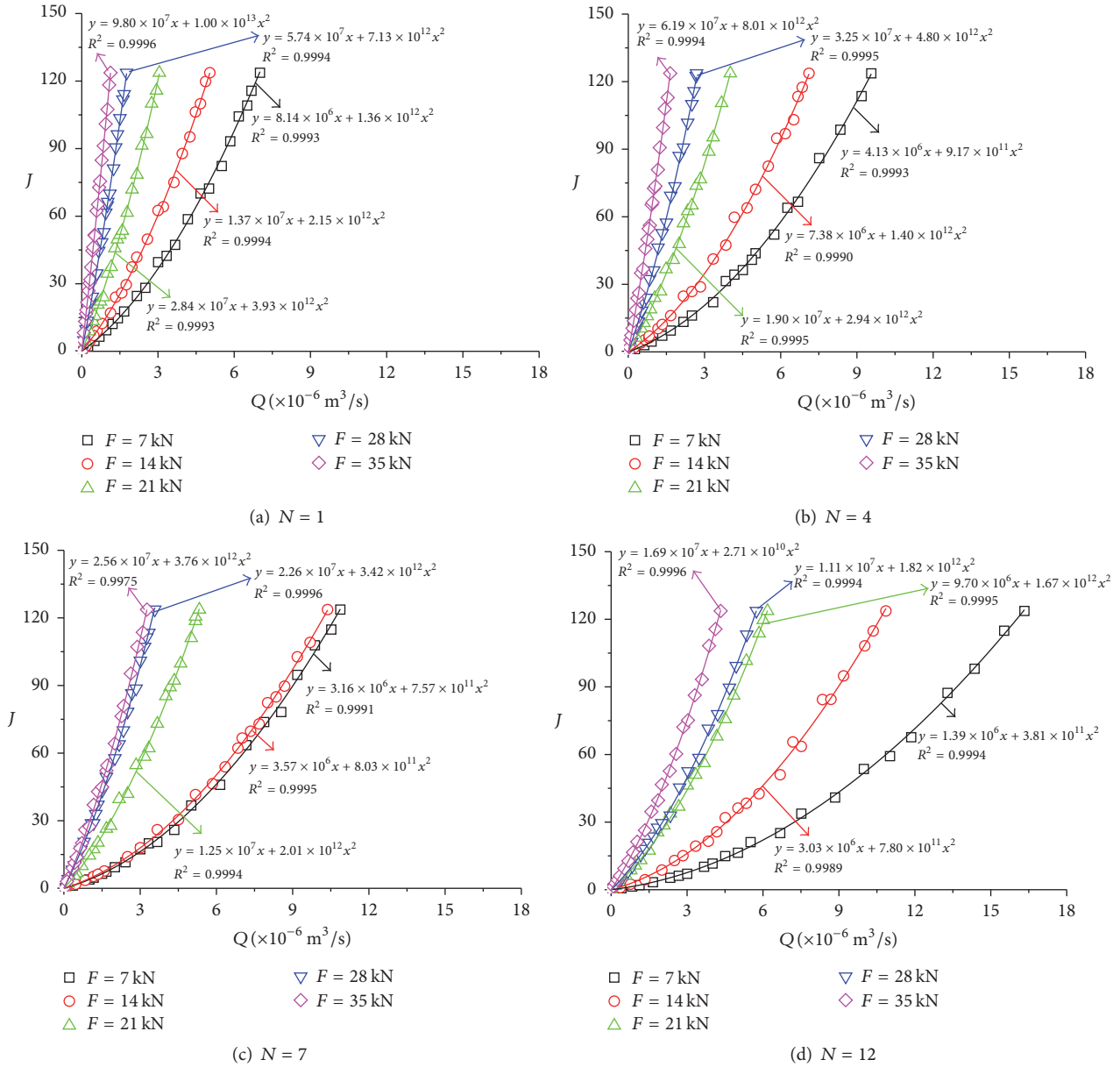

FIGURE 5: Regression analysis of hydraulic gradient as a function of measured flow rate using Forchheimer's law of fracture networks subjected to increased boundary loads.

as an example, as N increases from 1 to 12, b decreases by 71.91% (F = 7 kN), 63.67% (F = 14 kN), 57.51% (F = 21 kN), 74.47% (F = 28 kN), and 72.90% (F = 35 kN), respectively.

In view of the fact that the variations of linear and nonlinear coefficients a and b against N and F are very similar, b as a function of a was analyzed [29], as plotted in Figure 7(e). The experimental data can be fitted very well using the following empirical function:

$$b = 7.899 \times 10^6 a^{0.766}. \quad (14)$$

Although (14) fits very well the relationship between the coefficients a and b, with the generating R^2 of 0.9927, the applicability of this equation needs to be further verified.

To quantify the degree of the nonlinear effect of fluid flow through the fracture networks, variations of E for all test cases were calculated and plotted as a function of J based on (8), as shown in Figure 8. As J increases, E displays an increasing trend, while the rate of its increase steadily diminishes. The variation process can be well described using a power function

$$E = cJ^d, \quad (15)$$

where the fitting coefficients (c and d) are related to both the boundary load conditions and number of intersections. For a certain N, as F increases, the coefficient c shows a decreasing trend, but the coefficient d increases. However, at a given F,

Table 1: Values of a, b, J_c, and R^2 of fracture networks with different numbers of intersections N subjected to various boundary loads F.

N	F (kN)	a (kg·Pa^{-1}·s^{-1}·m^{-4})	b (kg·Pa^{-1}·m^{-7})	R^2	J_c
1	7	8.14E + 06	1.36E + 12	0.9993	6.01
	14	1.37E + 07	2.15E + 12	0.9994	10.78
	21	2.84E + 07	3.93E + 12	0.9993	25.34
	28	5.74E + 07	7.13E + 12	0.9994	57.05
	35	9.80E + 07	1.00E + 13	0.9996	118.57
4	7	4.13E + 06	9.17E + 11	0.9993	2.29
	14	7.38E + 06	1.40E + 12	0.9990	4.80
	21	1.90E + 07	2.94E + 12	0.9995	15.16
	28	3.25E + 07	4.80E + 12	0.9995	27.17
	35	6.19E + 07	8.01E + 12	0.9994	59.06
7	7	3.16E + 06	7.57E + 11	0.9991	1.63
	14	3.57E + 06	8.03E + 11	0.9995	1.96
	21	1.25E + 07	2.01E + 12	0.9994	9.58
	28	2.26E + 07	3.42E + 12	0.9996	18.44
	35	2.56E + 07	3.76E + 12	0.9975	21.50
12	7	1.39E + 06	3.81E + 11	0.9994	0.62
	14	3.03E + 06	7.80E + 11	0.9989	1.45
	21	9.70E + 06	1.67E + 12	0.9995	6.96
	28	1.11E + 07	1.82E + 12	0.9994	8.36
	35	1.69E + 07	2.71E + 12	0.9996	13.01

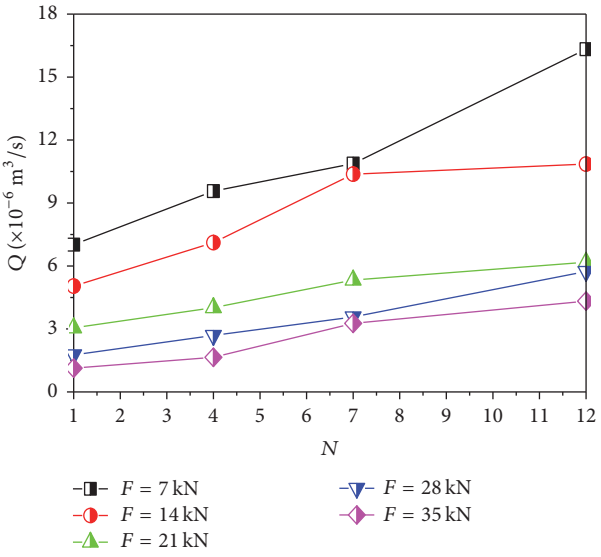

Figure 6: Q as a function of N for different F at a fixed J of 123.69.

with an increase in N, c plots an increasing trend while d decreases.

By defining a critical value of E = 0.1, J_c of the fracture networks with various numbers of intersections was calculated, as listed in Table 1. Figure 9 displays the changes in J_c due to the changes in N and F. As F increases, J_c shows an increasing trend. In the range of F from 7 to 35 kN, J_c increases by 6.35 times (N = 1), 7.73 times (N = 4), 3.97 times (N = 7), and 6.09 times (N = 12), respectively. The main reason for these variations may be as follows. For F_x = F_y, it is expected that the effect of normal loads plays a dominant role on the overall fluid flow field [42]. An increase in the normal load will undoubtedly lead to corresponding fracture closure. For each single fracture, a small change in fracture aperture can result in a large variation in the flow rate due to proportional relationships between Q and b_h^3 in (4), which would then impact J_c for the onset of flow transition. However, for a certain F, as N increases, J_c shows a decreasing trend. Taking F = 35 kN as an example, in the range of N from 1 to 12, J_c decreases from 118.57 to 13.01, or by 89.03%.

For fluid flow through fractured and porous media, the transmissivity has also been applied to estimate the nonlinear flow regime. Using (11), T of the fracture networks was calculated. Figure 10 shows the relationships between T and J. Notably, T is not a constant value but exhibits a decreasing trend with J, which further validates the existence of nonlinear flow behaviors in the fracture networks. With an increase in F, T decreases due to fracture closure. However, for a certain F, T shows an increasing trend with N. Using the least square method, J as a function of T can be well fitted with the following exponential function:

$$T = A + BC^J, \tag{16}$$

where the regression coefficients A, B, and C were all presented in Figure 10. The units of coefficients A and B are m^4 and C is a dimensionless constant.

When assessing the fluid flow through a single rock fracture, the Reynolds number (Re), which is defined as the ratio of inertial forces to viscous forces, is typically used to

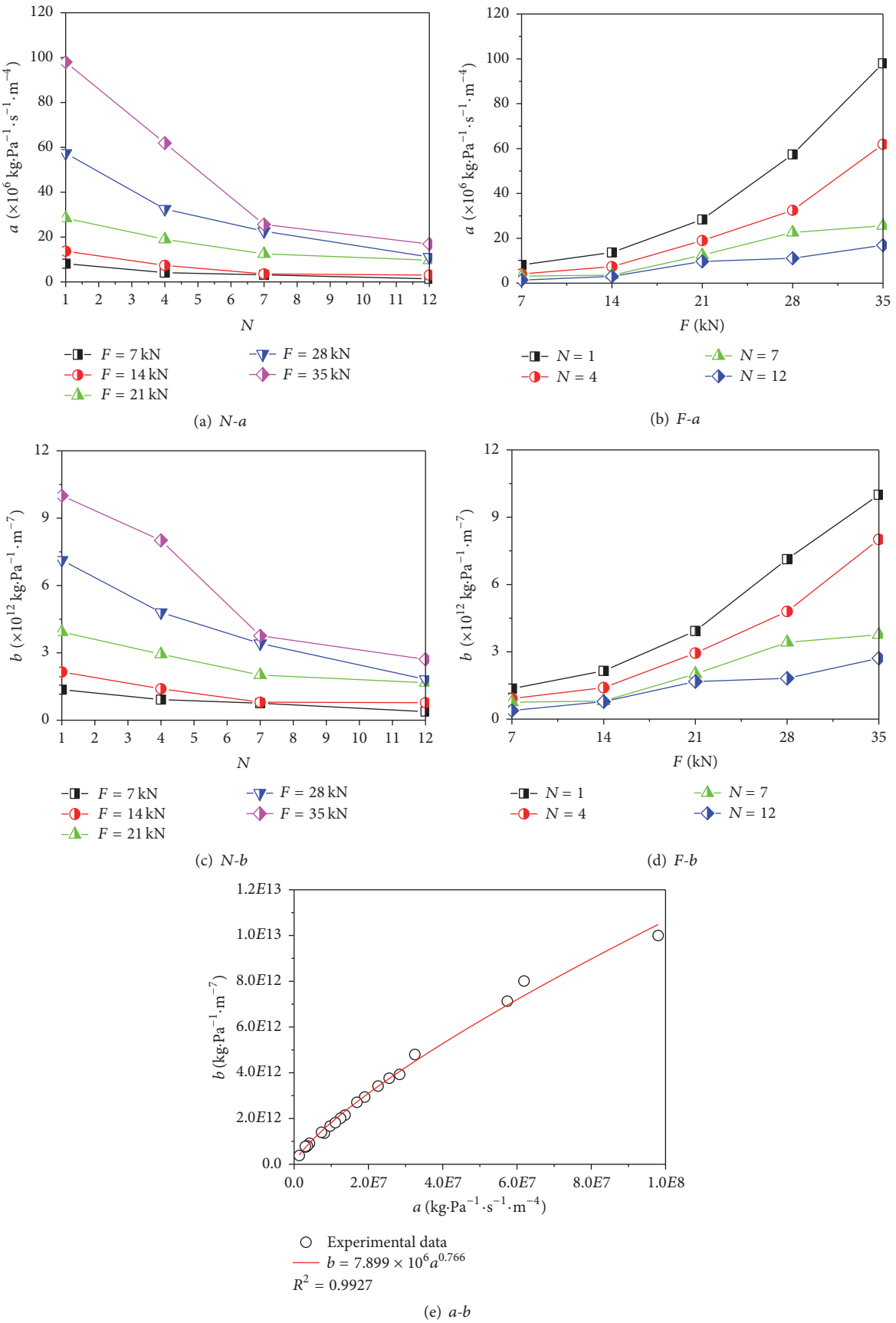

Figure 7: Variations in linear and nonlinear coefficients a and b, and the nonlinear relation between a and b.

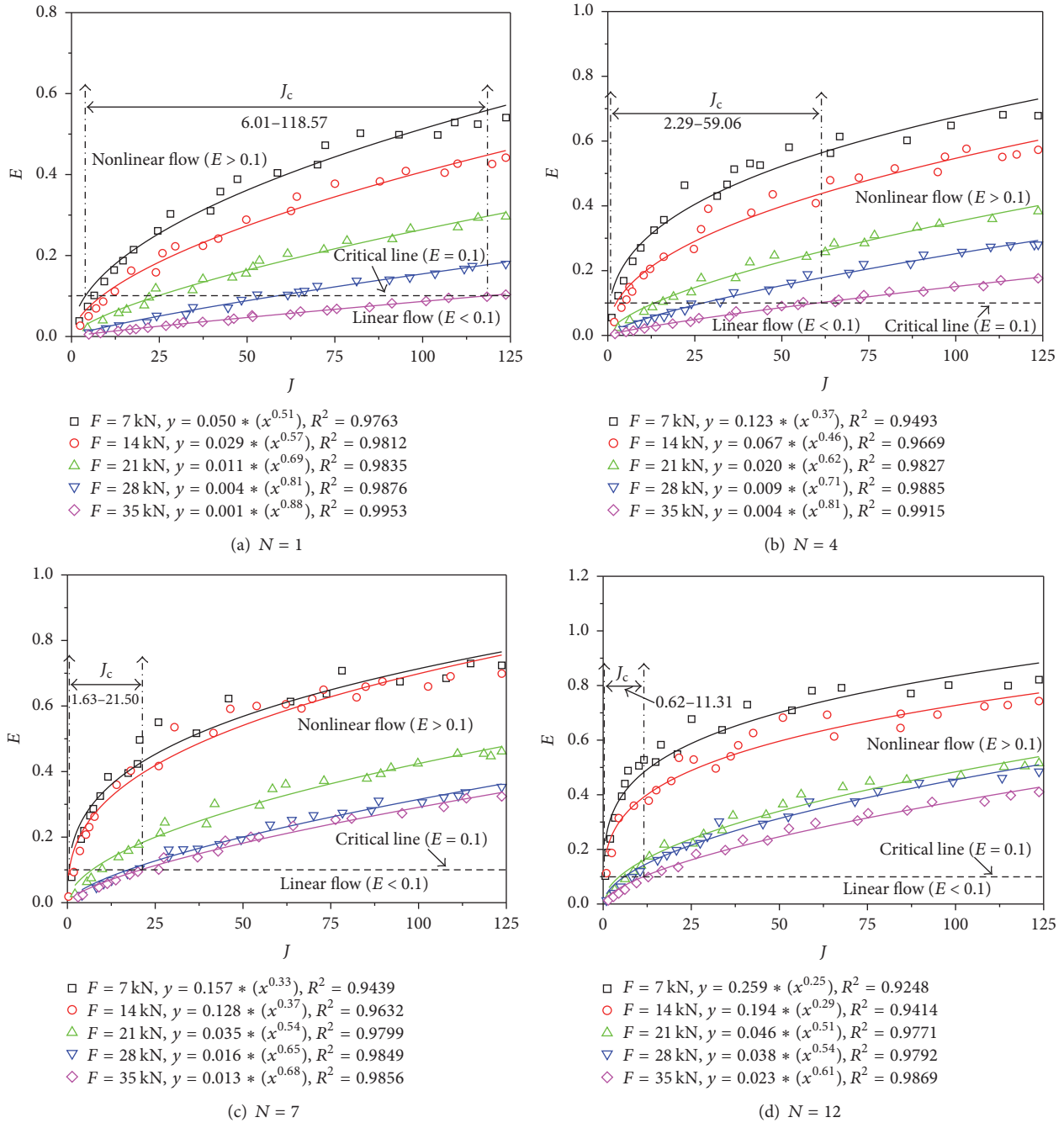

Figure 8: Evolution of nonlinear effect factor E with hydraulic gradient J.

quantify the onset of nonlinear flow. As noted above, the variations of normalized transmissivity (T/T_0) versus Re can be determined by extending the linear Darcy law with $T = \mu Q/(-\nabla P)$ [23, 25, 34, 43],

$$\frac{T}{T_0} = \frac{1}{1 + \beta \mathrm{Re}}, \tag{17}$$

where β is a dimensionless coefficient determined by the coefficients a and b in Forchheimer (6).

However, in engineering practices, there are hundreds to thousands of fractures, and the Re of each fracture generally cannot be ascertained. Instead, J in a model typically has known values and can be easily obtained. Therefore, in this study, the relationships between J and T/T_0 were used to evaluate the flow regimes in the fracture networks.

By fitting the experimental data sets, the relationships between J and T/T_0 for rock fracture networks in this study were analyzed, as shown in Figure 11. Here, T_0 denotes the

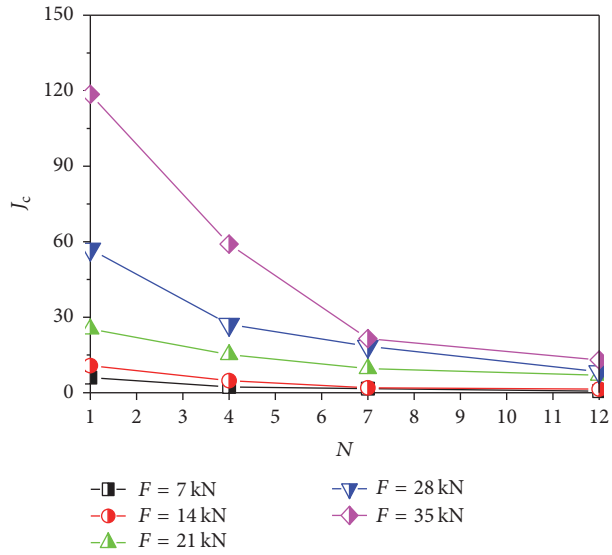

Figure 9: Relationships between J_c and N.

transmissivity corresponding to $J = 0$ in Figure 10, where the hydraulic head difference is sufficiently low and the inertial forces are negligible. The results show that variations in T/T_0 against J can be expressed as follows [14]:

$$\frac{T}{T_0} = 1 - \exp\left(-\alpha J^{-0.45}\right), \tag{18}$$

where α is a dimensionless coefficient. Note that the exponent of J is −0.45, which does not change with the number of intersections or boundary load conditions.

From Figure 11, as J increases, T/T_0 shows a decreasing trend. For a certain N, as F increases, the transmissivity relationships generally shift upward. However, for a certain F, the $J - T/T_0$ curves shift downward as N increases. In addition, the variations in T/T_0 with J can be divided into three stages. When J is small (i.e., less than 0.2), with the increase of J, T/T_0 approximately holds a constant value of 1.0; thus, the fluid flow is linear. Then, with continuously increasing J, T/T_0 decreases and the reduction rate of T/T_0 first increases and then decreases. Based on (12) and (18), when $T/T_0 = 0.9$, J_c is calculated, which is in the ranges 8.98–103.16 ($N = 1$), 3.46–61.40 ($N = 4$), 2.69–28.37 ($N = 7$), and 1.10–15.50 ($N = 12$), respectively. Generally, the range of J_c is larger than that calculated based on (6) and (8) shown in Figure 9.

The variations of the coefficient α with varying N and F are shown in Figure 12. For a certain N, as F increases, α increases. In the range of 7–35 kN, α generally increases by a factor of 2. However, at a given F, the coefficient α decreases with N. As N increases from 1 to 12, α shows a decrease of 61.14% ($F = 7$ kN), 66.37% ($F = 14$ kN), 42.98% ($F = 21$ kN), 55.29% ($F = 28$ kN), and 57.38% ($F = 35$ kN), respectively.

From the quadratic relationships between Q and J of the fracture networks displayed in Figure 5, at a given J, the increase in Q varies with both F and N, which leads to the changes in the equivalent permeability of the fracture networks. To assess the discharge capacity of the fracture networks, the x-directional equivalent permeability k of the fracture networks was calculated at a specified inlet hydraulic pressure of 0.05 MPa, with the corresponding J of 10.31. The fluid flow took place in fractures only and was calculated by the cubic law.

Calculations were made with the following equation, assuming no gravity term:

$$Q = A\frac{k}{\mu}\frac{\partial P}{\partial x}, \tag{19}$$

where A is the cross-sectional area.

The changes in the equivalent permeability of the fracture networks in terms of N and F are displayed in Figure 13. For a certain N, as F increases, k of the model region decreases. In the range of F from 7 to 35 kN, k decreases by 90.31% ($N = 1$), 90.87% ($N = 4$), 82.28% ($N = 7$), and 84.82% ($N = 12$), respectively. In addition, the F-k variation curves can be divided into two stages. As $F = 7$–21 kN, the permeability changes are sensitive. However, when $F > 21$ kN, k changes gradually and approaches constant values. The main reason for these variations may be as follows. As F increases, the effective stress σ_{fne} in the fractures increases, resulting in corresponding fracture closure. The overall volume flow rate decreases. As the fracture aperture continues to decrease until the residual fracture aperture, the equivalent permeability of the fracture networks generally retains a constant value. However, at a given F, the equivalent permeability k increases with N mainly due to richer connectivity in the fracture networks.

5. Conclusions

This paper experimentally examines the impacts of number of intersections ($N = 1$, 4, 7, and 12) on stress-dependent

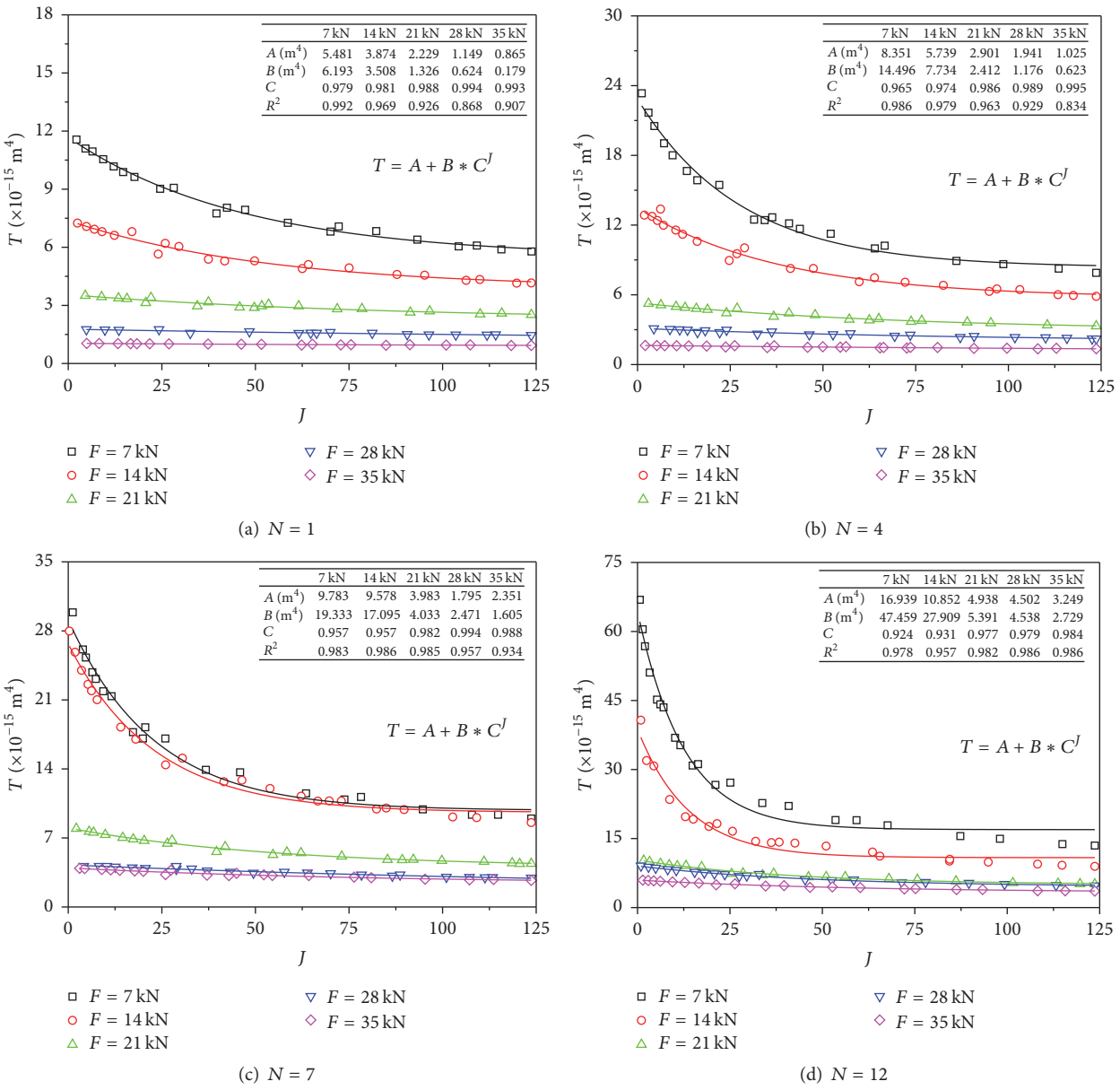

Figure 10: Regression analysis of transmissivity (T) as a function of hydraulic gradient J.

nonlinearity of fluid flow through real rock fracture networks. For each intersection number, a series of hydromechanical tests with respect to different inlet hydraulic pressures (0–0.6 MPa) and increasing boundary loads from 7 to 35 kN were conducted. The degree of nonlinearity, critical hydraulic gradient, normalized transmissivity, and the equivalent permeability of the fracture networks were all evaluated. The main conclusions are as follows:

(1) Forchheimer's law offers a good description for the relationships between volume flow rate and hydraulic gradient of water flow through the rock fracture networks. Both the linear coefficient a and nonlinear coefficient b in Forchheimer's law decrease with the number of intersections but increase with the boundary load. The changes of nonlinear coefficient b as a function of linear coefficient a can be well fitted using a power function $b = 7.899 \times 10^6 a^{0.766}$ based on the experimental data.

(2) The critical hydraulic gradient of the fracture networks is calculated by taking a critical nonlinear effect factor E value of 10%. With an increase in the number of intersections, the critical hydraulic gradient decreases mainly due to richer flowing pathways in the fracture networks. However, as the boundary load increases, the critical hydraulic gradient increases due to fracture closure caused by increasing effective

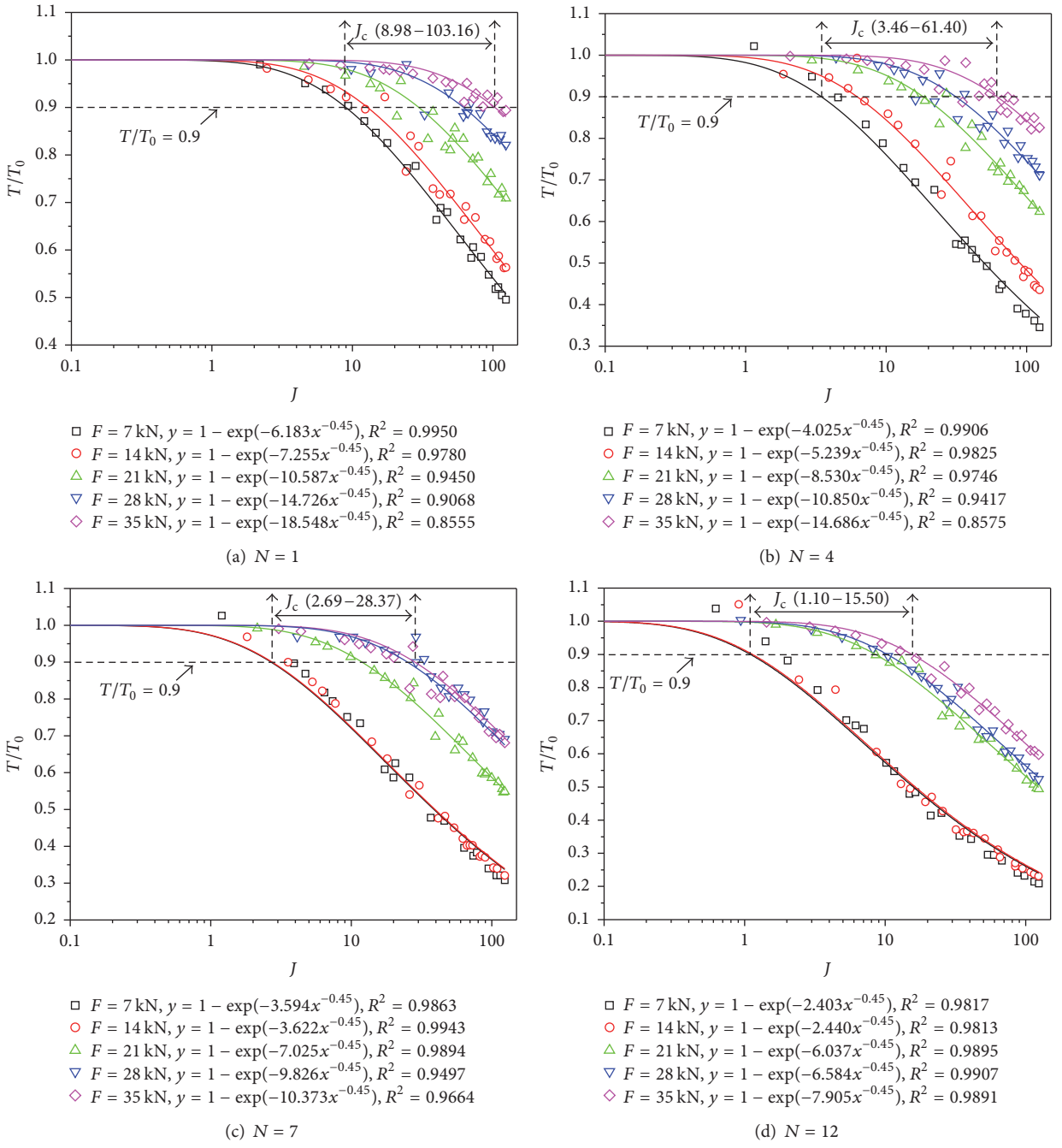

Figure 11: Relationships between hydraulic gradient J and the normalized transmissivity (T/T_0).

stress in the fractures. For all cases in this study, the critical hydraulic gradient is ranged between 0.62 and 118.57.

(3) With an increase in the hydraulic gradient, the transmissivity of the fracture networks displays an exponential decrease trend. In addition, the transmissivity increases with the number of intersections but decreases with the applied boundary load. The variations in normalized transmissivity as a function of hydraulic gradient were estimated with a mathematical expression $T/T_0 = 1 - \exp(-\alpha J^{-0.45})$. The coefficient α increases with the boundary load but decreases with the number of intersections. As the boundary load increases, the equivalent permeability of the fracture networks shows a decreasing trend.

Conflicts of Interest

The authors declare that they have no conflicts of interest.

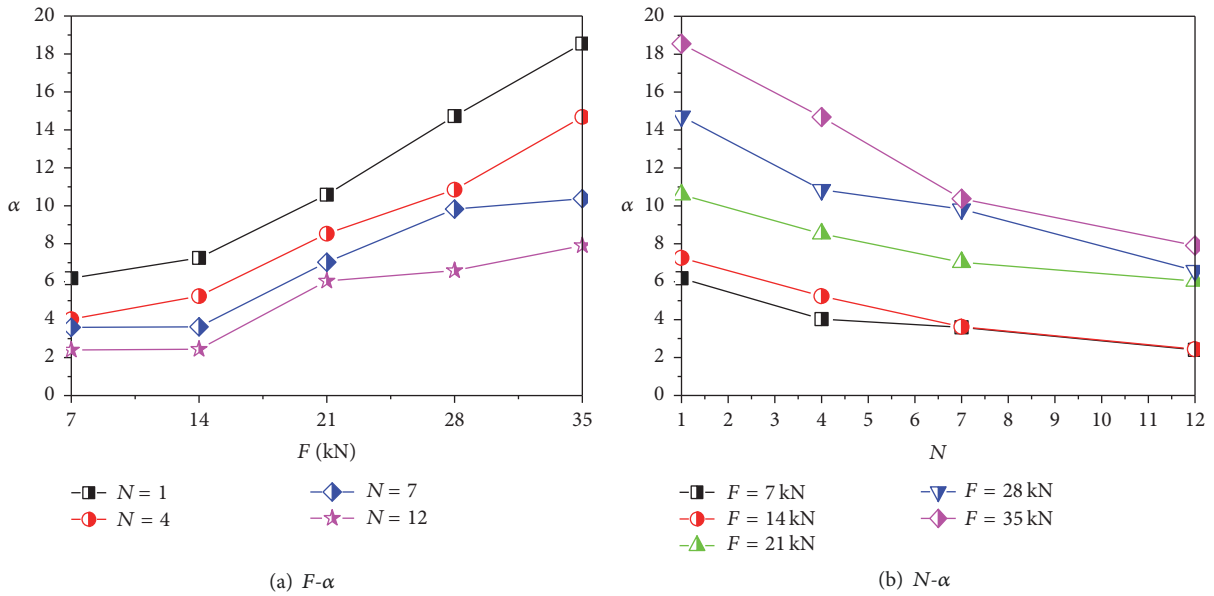

Figure 12: Variations in the coefficient α with varying N and F.

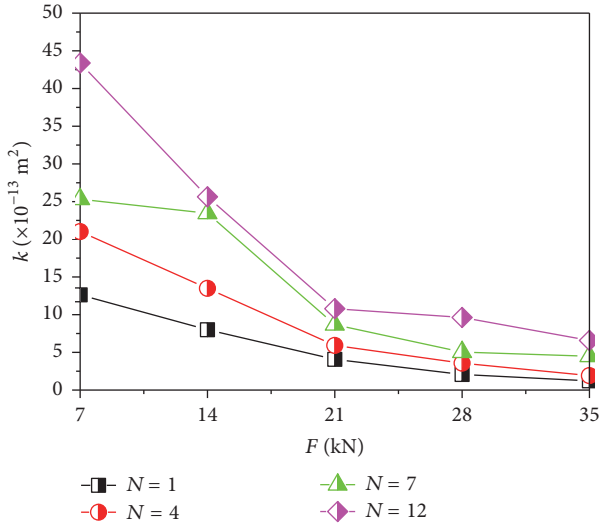

Figure 13: Equivalent permeability k changes due to the changes in F.

Acknowledgments

The financial support from the Fundamental Research Funds for the Central Universities, China (no. 2018QNA32), is gratefully acknowledged.

References

[1] M. Javadi, M. Sharifzadeh, K. Shahriar, and Y. Mitani, "Critical Reynolds number for nonlinear flow through rough-walled fractures: the role of shear processes," *Water Resources Research*, vol. 50, no. 2, pp. 1789–1804, 2014.

[2] L. P. Li, Z. Q. Zhou, S. C. Li, Z. Xu, and S. Shi, "An attribute synthetic evaluation system for risk assessment of floor water inrush in coal Mines," *Mine Water and the Environment*, vol. 34, no. 3, pp. 288–294, 2015.

[3] K. K. Singh, D. N. Singh, and P. G. Ranjith, "Laboratory simulation of flow through single fractured granite," *Rock Mechanics and Rock Engineering*, vol. 48, no. 3, pp. 987–1000, 2015.

[4] Y. Ju, Q. G. Zhang, Y. M. Yang, H. P. Xie, F. Gao, and H. J. Wang, "An experimental investigation on the mechanism of fluid flow through single rough fracture of rock," *Science China Technological Sciences*, vol. 56, no. 8, pp. 2070–2080, 2013.

[5] Q. Yin, H. Jing, H. Su, and H. Wang, "CO_2 permeability analysis of caprock containing a single fracture subject to coupled thermal-hydromechanical effects," *Mathematical Problems in Engineering*, vol. 2017, Article ID 1290748, 13 pages, 2017.

[6] J. Schmittbuhl, A. Steyer, L. Jouniaux, and R. Toussaint, "Fracture morphology and viscous transport," *International Journal of Rock Mechanics and Mining Sciences*, vol. 45, no. 3, pp. 422–430, 2008.

[7] A. Neuville, R. Toussaint, and J. Schmittbuhl, "Fracture roughness and thermal exchange: a case study at Soultz-sous-Forets," *Comptes Rendus - Geoscience*, vol. 342, no. 7-8, pp. 616–625, 2010.

[8] E. Huenges, T. Kohl, O. Kolditz, J. Bremer, M. Scheck-Wenderoth, and T. Vienken, "Geothermal energy systems: research perspective for domestic energy provision," *Environmental Earth Sciences*, vol. 70, no. 8, pp. 3927–3933, 2013.

[9] P. M. Quinn, B. L. Parker, and J. A. Cherry, "Using constant head step tests to determine hydraulic apertures in fractured rock," *Journal of Contaminant Hydrology*, vol. 126, no. 1-2, pp. 85–99, 2011.

[10] Y. Chen, S. Hu, K. Wei, R. Hu, C. Zhou, and L. Jing, "Experimental characterization and micromechanical modeling of damage-induced permeability variation in Beishan granite," *International Journal of Rock Mechanics and Mining Sciences*, vol. 71, pp. 64–76, 2014.

[11] J. Q. Zhou, S. H. Hu, S. Fang, Y. F. Chen, and C. B. Zhou, "Nonlinear flow behavior at low Reynolds numbers through rough-walled fractures subjected to normal compressive loading," *International Journal of Rock Mechanics and Mining Sciences*, vol. 80, pp. 202–218, 2015.

[12] P. A. Witherspoon, J. S. Y. Wang, K. Iwai, and J. E. Gale, "Validity of cubic law for fluid flow in a deformable rock fracture," *Water Resources Research*, vol. 16, no. 6, pp. 1016–1024, 1980.

[13] Y.-F. Chen, J.-Q. Zhou, S.-H. Hu, R. Hu, and C.-B. Zhou, "Evaluation of Forchheimer equation coefficients for non-Darcy flow in deformable rough-walled fractures," *Journal of Hydrology*, vol. 529, pp. 993–1006, 2015.

[14] R. Liu, L. Yu, and Y. Jiang, "Quantitative estimates of normalized transmissivity and the onset of nonlinear fluid flow through rough rock fractures," *Rock Mechanics and Rock Engineering*, vol. 50, no. 4, pp. 1063–1071, 2017.

[15] R. W. Zimmerman and G. S. Bodvarsson, "Hydraulic conductivity of rock fractures," *Transport in Porous Media*, vol. 23, no. 1, pp. 1–30, 1996.

[16] L. Wang, M. B. Cardenas, D. T. Slottke, R. A. Ketcham, and J. M. Sharp, "Modification of the Local Cubic Law of fracture flow for weak inertia, tortuosity, and roughness," *Water Resources Research*, vol. 51, no. 4, pp. 2064–2080, 2015.

[17] L. Yu, R. Liu, and Y. Jiang, "A review of critical conditions for the onset of nonlinear fluid flow in rock fractures," *Geofluids*, vol. 2017, Article ID 2176932, 17 pages, 2017.

[18] W. B. Durham and B. P. Bonner, "Self-propping and fluid flow in slightly offset joints at high effective pressures," *Journal of Geophysical Research: Atmospheres*, vol. 99, no. 5, pp. 9391–9399, 1994.

[19] H. Auradou, G. Drazer, A. Boschan, J.-P. Hulin, and J. Koplik, "Flow channeling in a single fracture induced by shear displacement," *Geothermics*, vol. 35, no. 5-6, pp. 576–588, 2006.

[20] A. Neuville, R. Toussaint, and J. Schmittbuhl, "Hydrothermal coupling in a self-affine rough fracture," *Physical Review E: Statistical, Nonlinear, and Soft Matter Physics*, vol. 82, no. 3, Article ID 036317, 2010.

[21] T. Babadagli, S. Raza, X. Ren, and K. Develi, "Effect of surface roughness and lithology on the water-gas and water-oil relative permeability ratios of oil-wet single fractures," *International Journal of Multiphase Flow*, vol. 75, pp. 68–81, 2015.

[22] R. Liu, B. Li, and Y. Jiang, "Critical hydraulic gradient for nonlinear flow through rock fracture networks: the roles of aperture, surface roughness, and number of intersections," *Advances in Water Resources*, vol. 88, pp. 53–65, 2016.

[23] R. W. Zimmerman, A. Al-Yaarubi, C. C. Pain, and C. A. Grattoni, "Non-linear regimes of fluid flow in rock fractures," *International Journal of Rock Mechanics and Mining Sciences*, vol. 41, no. 1, pp. 163–169, 2004.

[24] Z. Zhang and J. Nemcik, "Fluid flow regimes and nonlinear flow characteristics in deformable rock fractures," *Journal of Hydrology*, vol. 477, pp. 139–151, 2013.

[25] Q. Yin, G. Ma, H. Jing et al., "Hydraulic properties of 3D rough-walled fractures during shearing: an experimental study," *Journal of Hydrology*, vol. 555, pp. 169–184, 2017.

[26] K. G. Raven and J. E. Gale, "Water flow in a natural rock fracture as a function of stress and sample size," *International Journal of Rock Mechanics and Mining Sciences*, vol. 22, no. 4, pp. 251–261, 1985.

[27] T. Esaki, S. Du, Y. Mitani, K. Ikusada, and L. Jing, "Development of a shear-flow test apparatus and determination of coupled properties for a single rock joint," *International Journal of Rock Mechanics and Mining Sciences*, vol. 36, no. 5, pp. 641–650, 1999.

[28] B. Li, Y. J. Jiang, T. Koyama, L. R. Jing, and Y. Tanabashi, "Experimental study of the hydro-mechanical behavior of rock joints using a parallel-plate model containing contact areas and artificial fractures," *International Journal of Rock Mechanics and Mining Sciences*, vol. 45, no. 3, pp. 362–375, 2008.

[29] G. Rong, J. Yang, L. Cheng, and C. B. Zhou, "Laboratory investigation of nonlinear flow characteristics in rough fractures during shear process," *Journal of Hydrology*, vol. 541, pp. 1385–1394, 2016.

[30] D. J. Brush and N. R. Thomson, "Fluid flow in synthetic rough-walled fractures: navier-stokes, stokes, and local cubic law simulations," *Water Resources Research*, vol. 39, no. 4, pp. 1037–1041, 2003.

[31] L. Z. Xie, C. Gao, L. Ren, and C. B. Li, "Numerical investigation of geometrical and hydraulic properties in a single rock fracture during shear displacement with the Navier–Stokes equations," *Environmental Earth Sciences*, vol. 73, no. 11, article 28, pp. 7061–7074, 2015.

[32] J. Qian, H. Zhan, Z. Chen, and H. Ye, "Experimental study of solute transport under non-Darcian flow in a single fracture," *Journal of Hydrology*, vol. 399, no. 3-4, pp. 246–254, 2011.

[33] C. Cherubini, C. I. Giasi, and N. Pastore, "Bench scale laboratory tests to analyze non-linear flow in fractured media," *Hydrology and Earth System Sciences Discussions*, vol. 9, no. 4, pp. 2511–2522, 2012.

[34] M. Wang, Y.-F. Chen, G.-W. Ma, J.-Q. Zhou, and C.-B. Zhou, "Influence of surface roughness on nonlinear flow behaviors in 3D self-affine rough fractures: Lattice Boltzmann simulations," *Advances in Water Resources*, vol. 96, pp. 373–388, 2016.

[35] Z. Zeng and R. Grigg, "A criterion for non-darcy flow in porous media," *Transport in Porous Media*, vol. 63, no. 1, pp. 57–69, 2006.

[36] C. C. Xia, X. Qian, P. Lin, W. Xiao, and Y. Gui, "Experimental investigation of nonlinear flow characteristics of real rock joints under different contact conditions," *Journal of Hydraulic Engineering*, 2016.

[37] R. Olsson and N. Barton, "An improved model for hydromechanical coupling during shearing of rock joints," *International Journal of Rock Mechanics and Mining Sciences*, vol. 38, no. 3, pp. 317–329, 2001.

[38] ISRM, "Rock characterization, testing and monitoring—ISRM suggested methods," in *Suggested methods for the quantitative description of discontinuities in rock masses*, E. T. Brown, Ed., pp. 3–52, Pergamon, Oxford, 1981.

[39] R. Tse and D. M. Cruden, "Estimating joint roughness coefficients," *International Journal of Rock Mechanics and Mining Science and Geomechanics Abstracts*, vol. 16, no. 5, pp. 303–307, 1979.

[40] N. Barton, "Review of a new shear-strength criterion for rock joints," *Engineering Geology*, vol. 7, no. 4, pp. 287–332, 1973.

[41] N. Barton, S. Bandis, and K. Bakhtar, "Strength, deformation and conductivity coupling of rock joints," *International Journal of Rock Mechanics and Mining Sciences & Geomechanics Abstracts*, vol. 22, no. 3, pp. 121–140, 1985.

[42] K. B. Min, J. Rutqvist, C.-F. Tsang, and L. Jing, "Stress-dependent permeability of fractured rock masses: a numerical study," *International Journal of Rock Mechanics and Mining Sciences*, vol. 41, no. 7, pp. 1191–1210, 2004.

[43] P. G. Ranjith and W. Darlington, "Nonlinear single-phase flow in real rock joints," *Water Resources Research*, vol. 43, no. 9, pp. 146–156, 2007.